A&A 468, 1001–1008 (2007)
DOI: 10.1051/0004-6361:20066462

Astronomy & Astrophysics

A multiwavelength study of the ultracompact HII region associated with IRAS 20178+4046⋆

A. Tej[1], S. K. Ghosh[1], V. K. Kulkarni[2], D. K. Ojha[1], R. P. Verma[1], and S. Vig[1,⋆⋆]

[1] Tata Institute of Fundamental Research, Homi Bhabha Road, Colaba, Mumbai 400 005, India
e-mail: tej@tifr.res.in
[2] National Centre for Radio Astrophysics, Post Bag 3, Ganeshkhind, Pune 411 007, India

Received 27 September 2006 / Accepted 27 February 2007

ABSTRACT

Aims. We present a multiwavelength study of the ultra compact HII region associated with IRAS 20178+4046. This enables us to probe the different components associated with this massive star-forming region.
Methods. The radio emission from the ionized gas was mapped at 610 and 1280 MHz using the Giant Metrewave Radio Telescope (GMRT), India. We used 2MASS JHK_s data to study the nature of the embedded sources associated with IRAS 20178+4046. Submillimetre emission from the cold dust at 450 and 850 μm was studied using JCMT-SCUBA.
Results. The high-resolution radio continuum maps at 610 and 1280 MHz display compact spherical morphology. The spectral type of the exciting source is estimated to be ∼B0.5 from the radio flux densities. However, the near-infrared data suggest the presence of several massive stars (spectral type earlier than O9) within the compact ionized region. Submillimetre emission shows two dense cloud cores that are probably at different evolutionary stages. The total mass of the cloud is estimated to be ∼700–1500 $M_\odot$ from the submillimetre emission at 450 and 850 μm.
Conclusions. The multiwavelength study of this star-forming complex reveals an interesting scenario where we possibly see different evolutionary stages in star formation. The ultra compact HII region coinciding with the southern cloud core is at a later stage of evolution compared to the northern core, which is likely to be a protocluster.

Key words. infrared: ISM – radio continuum: ISM – ISM: HII regions – ISM: individual objects: IRAS 20178+4046

1. Introduction

The early stages and evolution of massive stars are some of the least understood aspects of star formation. Ultracompact (UC) HII regions are manifestations of newly formed massive (O or early B) stars deeply embedded in the parental cloud. IRAS 20178+4046 (G78.44+2.66) is a massive star-forming region chosen from the catalog of massive young stellar objects by Chan et al. (1996). It has been classified as a UC HII region (Kurtz et al. 1994, 1999). The kinematic distance estimates range from 1.5 kpc to 3.3 kpc (Kurtz et al. 1994; Caswell et al. 1975). In this paper we assume a distance of 3.3 kpc. The far-infrared (FIR) luminosity from the IRAS fluxes is estimated to be 7.0×10^4 $L_\odot$ (Kurtz et al. 1994). The IRAS low-resolution spectra (LRS) show a red continuum beyond ∼13 μm with the polycyclic aromatic hydrocarbon (PAH) feature at 11.3 μm (Volk & Cohen 1989). In their study of UC HII regions, Faison et al. (1998) present the intermediate-resolution infrared spectra of IRAS 20178+4046, where PAH features at 3.3, 8.7, and 11.3 μm, the [Ne II] line at 12.8 μm, and the silicate feature at 9.7 μm have been detected. The MSX mid-infrared (MIR) image at 21 μm is presented by Crowther & Conti (2003).

In a recent study, Verma et al. (2003) mapped this source in two FIR bands (∼150 and 210 μm) with the 1 m TIFR balloon-borne telescope. They also present the ISO observations using the ISOCAM instrument in seven spectral bands (3.30, 3.72, 6.00, 6.75, 7.75, 9.62, and 11.4 μm). The ISOCAM images mainly consist of a single component with a lobe toward south. They modelled this source with a single core and a dust density distribution of the form r^{-2} comprised mainly of silicates. IRAS 20178+4046 has been part of several maser surveys (Codella et al. 1996; Baudry et al. 1997; Slysh et al. 1999; Szymczak et al. 2000), but no maser has been found to be associated with this source. It was detected in the CS(2–1) survey of Bronfman et al. (1996). McCutcheon et al. (1991), and Wilking et al. (1989) observed this source in the CO lines as part of the survey of protostellar candidates.

In this paper, we present a multiwavelength study of this UC HII region. In Sect. 2, we describe the radio continuum observations and the related data-reduction procedure used. In this section, we also discuss other available datasets used in the present study. Section 3 presents a comprehensive discussion of the results obtained. In Sect. 4, we discuss the general star-forming scenario in the region associated with IRAS 20178+4046 and in Sect. 5 we summarise the results.

2. Observations, data reduction and other available datasets

2.1. Radio continuum observations

To probe the ionized gas component, radio continuum interferometric mapping of the region around IRAS 20178+4046 was carried out using the Giant Metrewave Radio Telescope

⋆ GMRT data is only available in electronic form at the CDS via anonymous ftp to cdsarc.u-strasbg.fr (130.79.128.5) or via http://cdsweb.u-strasbg.fr/cgi-bin/qcat?J/A+A/468/1001
⋆⋆ *Present address*: INAF - Osservatorio Astrofisico di Arcetri, Largo E. Fermi, 51-50125, Italy.

(GMRT) array, India. Observations were carried out at 1280 and 610 MHz. The GMRT has a "Y"-shaped hybrid configuration of 30 antennas, each 45 m in diameter. There are six antennas along each of the three arms (with arm length of ~14 km). These provide high angular resolution (longest baseline ~25 km). The rest of the twelve antennas are located in a random and compact arrangement within 1×1 km^2 near the centre and is sensitive to large-scale diffuse emission (shortest baseline ~100 m). Details of the GMRT antennas and their configurations can be found in Swarup et al. (1991). The radio sources 3C 48 and 3C 286 were used as the primary flux calibrators, while 2052+365 was used as the phase calibrator for both the 1280 and 610 MHz observations.

Data were reduced using AIPS. The data sets were carefully checked using tasks UVPLT and VPLOT for bad data (owing to dead antennas, bad baselines, interference, spikes, etc.). Subsequent editing was carried out using the tasks UVFLG and TVFLG. Maps of the field were generated by Fourier inversion and subsequent cleaning using the task IMAGR. Several iterations of self calibration were carried out to obtain improved maps.

2.2. Other available datasets

2.2.1. Near-infrared data from 2MASS

Near-infrared (NIR) (JHK_s) data for point sources around IRAS 20178+4046 were obtained from the Two Micron All Sky Survey[1] (2MASS) Point Source Catalog (PSC). Source selection was based on the "read-flag" that gives the uncertainties in the magnitudes. In our sample we retain only those sources for which the "read-flag" values are 1–3. The 2MASS data were used to study the sources associated with the UC HII region.

2.2.2. Mid-infrared data from MSX

The Midcourse Space Experiment[2] (MSX) surveyed the Galactic plane in four MIR bands centred at 8.3 (A), 12.13 (C), 14.65 (D), and 21.34 μm (E) at a spatial resolution of ~18″ (Price et al. 2001). The MIR data were used to model the continuum SED from the interstellar medium around IRAS 20178+4046. Other than this, two of the MSX bands (A and C) cover the unidentified infrared bands (UIBs) at 6.2, 7.7, 8.7, 11.3, and 12.7 μm. The MSX images in the four bands for the region around IRAS 20178+4046 were used to study the emission from the UIBs and to estimate the spatial distribution of temperature and optical depth of the warm interstellar dust. The MSX Point Source Catalog (MSX PSC) was used to study MIR sources associated with the UC HII region.

2.2.3. Sub-mm data from JCMT

Submillimetre observations at 450 and 850 μm using the Submillimetre Common-User Bolometer Array (SCUBA) instrument of the James Clerk Maxwell Telescope[3] (JCMT) were retrieved from the JCMT archives and processed using their standard pipeline SCUBA User Reduction Facility (SURF). The JCMT-SCUBA observations for the data used in our study were carried out on 17 Aug. 1998. Uranus was used as the primary flux calibrator for the maps. The submillimetre maps were used to study the cold-dust environment associated with IRAS 20178+4046.

3. Results and discussion

3.1. Radio continuum emission from ionized gas

High-resolution radio maps were generated from the GMRT data. The radio continuum emission from the ionized gas associated with the region around IRAS 20178+4046 at 1280 and 610 MHz is shown in Fig. 1. The details of the observations and maps are given in Table 1. For the 610 MHz observations, we present the map generated by using only baselines larger than 1 kilo-lambda. Correction factors for the system temperature (T_{sys}) were obtained from additional observations of the neighbouring sky on and off the Galactic plane. The correction factors are 1.2 and 1.6 for 1280 and 610 MHz, respectively. The generated maps were scaled using the T_{sys} correction factors obtained from our observations. The integrated flux densities from our maps at 1280 and 610 MHz are 57 ± 4 and 66 ± 4 mJy, respectively. The flux densities are estimated by integrating down to the lowest selected contour at the 3σ level, where σ-s are the rms noises in the respective maps. The corresponding size of the UC HII region is ~10″ and 15″ at 1280 and 610 MHz, respectively. Considering the errors, these flux densities are consistent with the hypothesis that the emission at these frequencies are optically thin. For this UC HII region, Wilking et al. (1989) estimate flux density values of 80 and 65 mJy from their 15 and 5 GHz radio maps and McCutcheon et al. (1991) obtain a value of 69 mJy at 5 GHz. As expected from our low-frequency GMRT data, the 5 GHz flux density values of the above studies also indicate an optically thin continuum flux distribution. The higher value at 15 GHz from Wilking et al. (1989) may be due to the contribution from the extended emission.

Kurtz et al. (1994, 1999) have also studied this source at 8.3 and 15 GHz. Kurtz et al. (1994) estimate flux density values of 82.2 and 35.6 mJy from their very high-resolution (<1″) maps using the VLA B array at 8.3 and 15 GHz, respectively. The integration boxes used by them are $9\farcs4 \times 8\farcs9$ and $9\farcs5 \times 8\farcs5$ for the two bands. Later observations by Kurtz et al. (1999) at 8.3 GHz with the VLA D array give a value of 68 and 158 mJy for 50″ and 300″ boxes, respectively with a synthesized beam size of $8\farcs7 \times 7\farcs8$. It should be noted here that the 300″ box covers a much larger area and includes the surrounding extended diffuse emission.

The contour maps at 1280 and 610 MHz generated from the GMRT observations display a simple compact spherical morphology. In comparison, the high-resolution (<1″) radio map at

[1] This publication makes use of data products from the Two Micron All Sky Survey, which is a joint project of the University of Massachusetts and the Infrared Processing and Analysis Center/California Institute of Technology, funded by the NASA and NSF.

[2] This research made use of data products from the Midcourse Space Experiment. Processing of the data was funded by the Ballistic Missile Defense Organization with additional support from the NASA Office of Space Science. This research also made use of the NASA/ IPAC Infrared Science Archive, which is operated by the Jet Propulsion Laboratory, Caltech, under contract with the NASA.

[3] This paper makes use of data from the James Clerk Maxwell Telescope Archive. The JCMT is operated by the Joint Astronomy Centre on behalf of the UK particle Physics and Astronomy Research Council, the National Research Council of Canada, and The Netherlands Organisation for Pure Research.

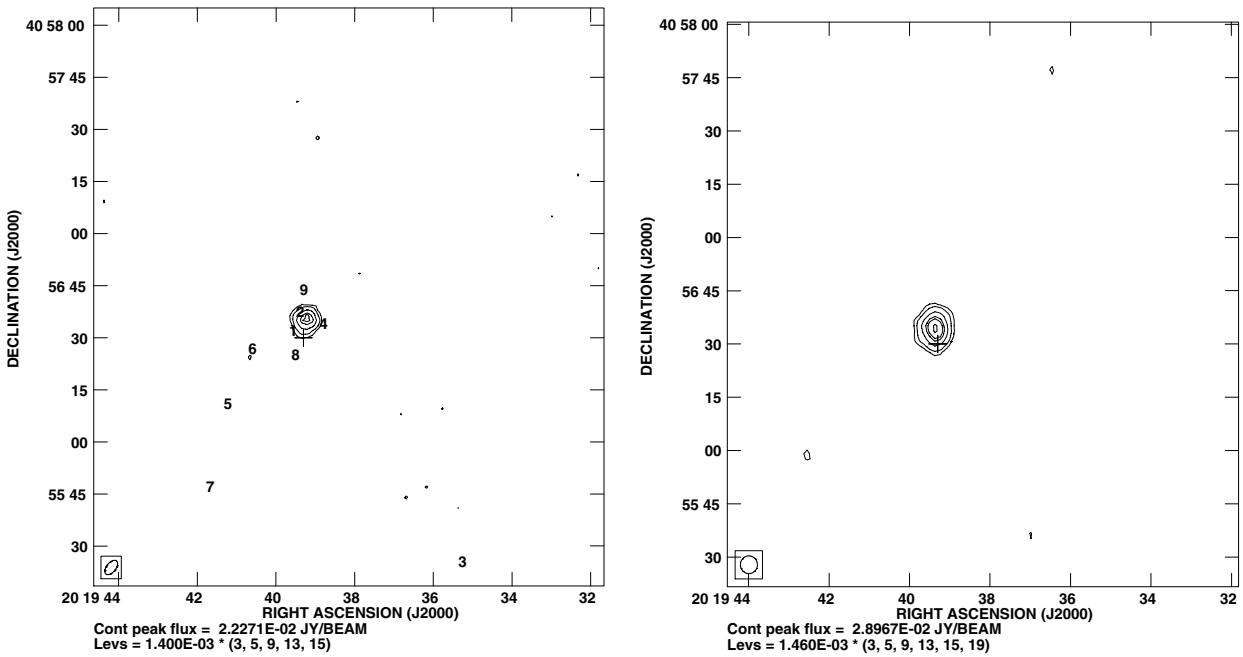

Fig. 1. High-resolution radio continuum maps at 1280 MHz (*left*) and 610 MHz (*right*) for the region around IRAS 20178+4046. The rms noises are ∼1.4 and 1.5 mJy/beam and the synthesized beam sizes are 4.″9 × 2.″7 and 5.″0 × 4.″8 at 1280 and 610 MHz, respectively. 2MASS sources with spectral type estimations earlier than B0.5 (see Sect. 3.2) are marked on the 1280 MHz map. The plus sign marks the position of the IRAS point source.

Table 1. Details of the radio interferometric continuum observations of the ionized region associated with IRAS 20178+4046.

Details	1280 MHz	610 MHz
Date of Obs.	2 Aug. 2003	18 Sep. 2004
Primary beam	26′	54′
Cont. bandwidth (MHz)	16	16
Synth. beam	4.″9 × 2.″7	5.″0×4.″8†
Position angle (deg)	–38.6	–0.25
Peak flux (mJy/beam)	22.3	29.0
rms noise (σ)(mJy/beam)	1.4	1.5
Largest detectable scale size	∼8′	∼17′
Highest angular resolution	∼2″	∼4″
Int. flux density‡ (mJy)	57 ± 4	66 ± 4

† For 610 MHz, the synthesized beam size is for the baselines >1 kilo-lambda.
‡ Flux densities are obtained by integrating down to the contour at 3σ level, where σ represents the map noise in the corresponding frequency band.

8.3 GHz of Kurtz et al. (1994) shows a cometary UC HII region. However, the sources are resolved out in their 15 GHz map and morphology looks "clumpy". This is possibly the reason for the low integrated flux density (35.6 mJy) obtained at this frequency. The lower resolution (8.″7 × 7.″8) 8.3 GHz map by Kurtz et al. (1999) is unresolved with an extended east-west emission seen to the south, which is unlikely to be connected with the UC HII region according to the authors. A point worth mentioning here is that we possibly detect extended diffuse emission in the low-resolution map at 610 MHz (not presented in this paper). But the signal-to-noise ratio of the map is not sufficient to conclusively comment on the nature and association if any of this extended diffuse emission with the UC HII region. However, we do not detect any such emission in our 1280 MHz map. This could be because the flux levels of the extended emission are below our sensitivity limit at 1280 MHz.

Using the low-frequency flux densities at 1280 and 610 MHz from our GMRT observations and the 8.3 GHz data from Kurtz et al. (1999), we derived the physical properties of the compact core of the HII region associated with IRAS 20178+4046. Mezger & Henderson (1967) have shown that, for a homogeneous and spherically symmetric core, the flux density can be written as

$$S = 3.07 \times 10^{-2} T_{\rm e} \nu^2 \Omega (1 - {\rm e}^{-\tau(\nu)}), \quad (1)$$

where

$$\tau(\nu) = 1.643 a \times 10^5 \nu^{-2.1} (EM) T_{\rm e}^{-1.35}, \quad (2)$$

where S is the integrated flux density in Jy, $T_{\rm e}$ the electron temperature in K, ν the frequency of observation in MHz, τ the optical depth, Ω the solid angle subtended by the source in steradians, and EM the emission measure in cm^{-6} pc. Also, a is a correction factor, and we used a value of 0.99 (using Table 6 of Mezger & Henderson 1967) for the frequency range 0.6–8 GHz and $T_{\rm e}$ = 8000 K. The two GMRT maps were convolved to a common angular resolution of 8.″7 × 7.″8, which is the resolution of the 8.3 GHz map of Kurtz et al. (1999). In our case, since the core is unresolved, Ω is taken as this synthesized convolved beam size (i.e $\Omega = 1.133 \times \theta_a \times \theta_b$, where θ_a and θ_b are the half-power beam sizes). The peak flux densities of the core in the 0.6–8.3 GHz frequency range are consistent with an optically thin HII region. Assuming a typical electron temperature of 8000 K, these flux densities were used to fit the above equations. The best-fit value for the emission measure is 2.9 ± 0.6 × 10^5 cm^{-6} pc. We obtained an estimate of 1.4 × 10^3 cm^{-3} for the electron density of $n_{\rm e} = (EM/r)^{0.5}$, with r being the core size, which in this case corresponds to the synthesized convolved beam size of 8.″7 × 7.″8. These values are lower compared to the estimates of Kurtz et al. (1994) obtained from

their high-resolution maps at 8.3 GHz. They derive values of 2×10^6 cm^{-6} pc and 5.2×10^3 cm^{-3} for EM and n_e, respectively. It should be noted here that the beam size of Kurtz et al. (1994) is much smaller than the convolved beam size used in our derivation.

Taking the total integrated flux densities of 57 and 66 mJy estimated from the 1280 and 610 MHz maps and using the formulation of Schraml & Mezger (1969) and the table from Panagia (1973; Table II), we estimate the exciting zero-age main-sequence star (ZAMS) of this UC HII region to be of spectral type B0.5–B0. This is consistent with the estimates of Kurtz et al. (1994, 1999). However, the FIR luminosity of 7.0×10^4 $L_\odot$ from IRAS PSC implies an exciting star of spectral type O8 (Kurtz et al. 1994). Radiative transfer modelling of the FIR and MIR flux densities of IRAS 20178+4046 by Verma et al. (2003) also suggests an O7 ZAMS exciting star. In a later section (see Sect. 3.4), a detailed model of the emission from the ISM around IRAS 20178+4046 has been presented, which implies the region to be powered by a cluster with the most massive star being of type B0.

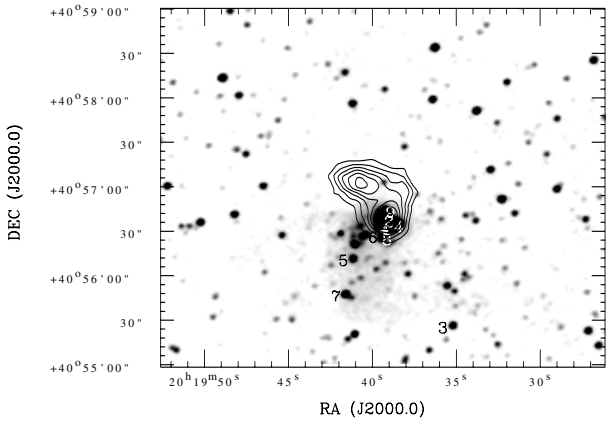

Fig. 2. The 2MASS K_s-band image. Overplotted are the massive stars within the diffuse emission associated with the UC HII region IRAS 20178+4046 (see discussion on the CM diagrams) The plus sign represents the IRAS point source position. Contour map of the dust emission at 850 μm is also overlaid (see Sect. 3.3).

3.2. Embedded cluster in the near-infrared

The 2MASS K_s-band image of the region around IRAS 20178+4046 is shown in Fig. 2. We see the presence of a stellar group/cluster mostly concentrated around the UC HII region. We used the 2MASS JHK_s data to study the nature of these sources seen in the vicinity of this UC HII region associated with IRAS 20178+4046. We selected a large area of 90″ radius centred on the IRAS point source so as to completely cover the UC HII region and the surrounding diffuse nebulosity seen in the near-infrared images. We restricted our sample of sources to those with good quality photometry (2MASS "read-flag" 1–3). Figure 3 shows the two $((J-H)/J$ and $(H-K)/K)$ NIR colour–magnitude (CM) diagrams. Using the ZAMS loci and the reddening vectors, we estimated the spectral type of the sources. The two CM diagrams show the presence of nine early type sources with spectral types ∼B0.5 or earlier, out of which six sources are common to both diagrams. Within an error of around one subclass (except for source #3), the spectral type estimations derived from both the CM diagrams are consistent. It is likely that the source #3 (which has the least extinction among the early type stars) is a foreground star, though it is not very close to the zero extinction curve. It is also possible that it does not belong to the group, because spatially it is farther away (see Fig. 2). The nine early type sources identified from both the CM diagrams are listed in Table 2.

Figure 4 shows the colour–colour (CC) diagram for the sources in the region associated with IRAS 20178+4046. For clarity we classified the CC diagram into three regions (e.g. Tej et al. 2006; Ojha et al. 2004a,b). The sources in region "F" are generally considered to be either field stars, Class III objects, or Class II objects with small NIR excess. The "T" sources are classical T Tauri stars (Class II objects) with large NIR excess or Herbig AeBe stars with small NIR excess. The "P" region has mostly protostar-like Class I objects and Herbig AeBe stars. Considering the quoted magnitude errors in Table 2, the majority of the early type sources (except source #6 and #3) are seen to lie in the "T" region.

In Fig. 2, we have overplotted sources listed in Table 2 on the K_s-band 2MASS image. It is interesting to see that five of these massive stars form a cluster at the centre, of which the position of source #1 coincides with the IRAS point source position. Compared with the radio morphology (Fig. 1 left panel), sources #1 and #2 are well within the compact ionized region. Sources #4, #6, #8, #9 envelope the UC HII region almost in a ring like structure. Apart from this clustering, three sources (#6, #5, #7) form a tail-type arc extending to the south. They lie within the diffuse emission (southward lobe) seen in the K_s-band image.

The presence of this massive star clustering makes the complex interesting because the radio flux density suggests a B0–B0.5 exciting source. It is likely that these sources are deeply embedded. This results in absorption of a large fraction of UV photons by the surrounding dust, which results in the underestimation of the spectral type from the radio flux density of the ionized gas. Star #2 has spectral type much earlier than O5 as indicated by both the CM diagrams. This could either be a deeply embedded pre-main-sequence (PMS) star or two or more unresolved early-type stars. However, there is a discrepancy in the FIR luminosity (Kurtz et al. 1994) when compared with the total luminosity derived from the NIR sources. This could probably be due to the distance uncertainties, IR excess, and 2MASS resolution limit, which results in inaccuracies in the spectral type determinations from the NIR CM diagrams. Hence, additional infrared spectroscopic observations are essential for determining the exact nature and spectral type of these sources.

3.3. Dust emission in the sub-mm from JCMT-SCUBA data

We used the emission in submillimetre wavebands to study the cold-dust environment in the region around IRAS 20178+4046. The spatial distribution of cold-dust emission at 450 and 850 μm is displayed in Fig. 5. The angular resolutions are 8.″8 and 14.″0 for the 450 and 850 μm wave bands, respectively. The 450 μm map is relatively noisy and shows a clumpy nature, whereas the 850 μm map clearly shows the presence of two dust cores.

The dust mass can be estimated from the following relation:

$$M_{\rm dust} = 1.88 \times 10^{-4} \left(\frac{1200}{\nu}\right)^{3+\beta} S_\nu (e^{0.048\nu/T_{\rm d}} - 1) d^2. \quad (3)$$

This is taken from Sandell (2000) and is a simplified version of Eq. (6) in Hildebrand (1983). The above equation assumes the standard Hildebrand opacities (i.e. $\kappa_{1200\ \rm GHz} = 0.1$ cm^2 g^{-1}). Here, S_ν is the flux density at frequency ν, $T_{\rm d}$ the dust temperature, β the dust emissivity index that is taken to be 2

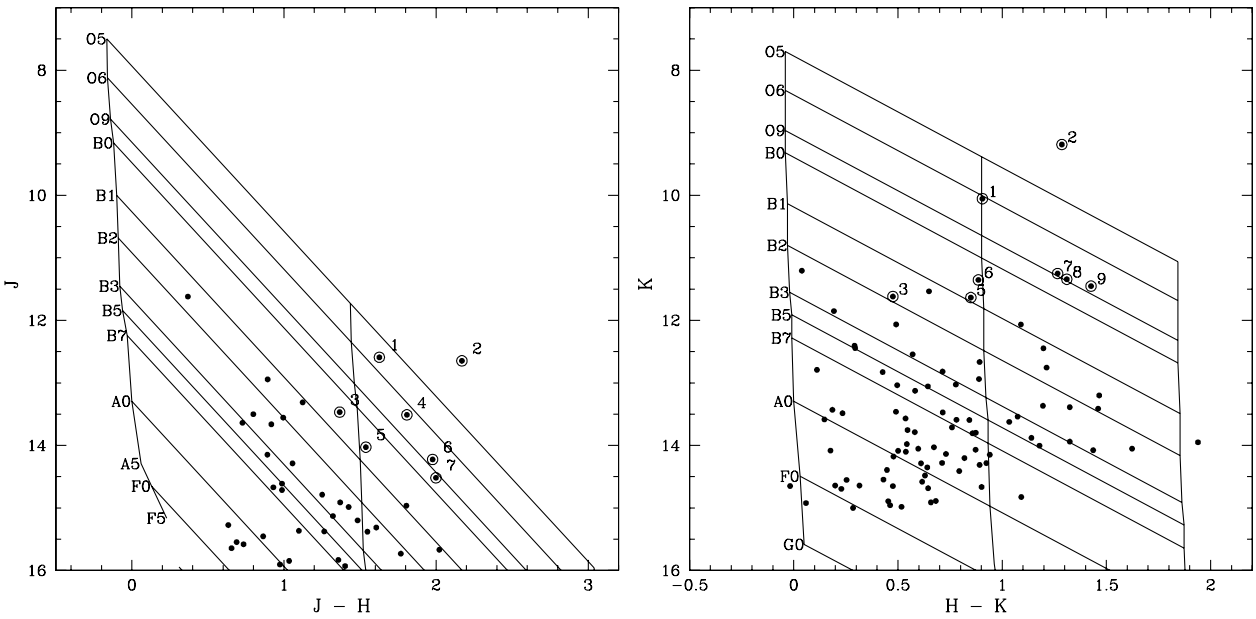

Fig. 3. Colour–magnitude diagrams of the infrared cluster in the IRAS 20178+4046 region. The nearly vertical solid lines represent the zero age main sequence (ZAMS) loci with 0, 15, and 30 mag of visual extinction corrected for the distance. The slanting lines show the reddening vectors for each spectral type. The magnitudes and the ZAMS loci are all plotted in the Bessell & Brett (1988) system.

Table 2. Early type sources (∼B0.5 and earlier) from the NIR CM diagram of IRAS 20178+4046.

Source No.	RA (2000.0) (hh:mm:ss.s)	Dec (2000.0) (dd:mm:ss.s)	J (mag)	H (mag)	K_s (mag)
1	20:19:39.5	+40:56:30.5	12.491 ± 0.034	10.929 ± 0.023	10.016 ± 0.027
2	20:19:39.3	+40:56:35.9	12.532 ± 0.030	10.433 ± 0.039	9.150 ± 0.029
3	20:19:35.2	+40:55:24.0	13.380 ± 0.022	12.076 ± 0.019	11.580 ± 0.015
4	20:19:38.7	+40:56:32.6	13.400 ± 0.040	11.659 ± 0.034	–
5	20:19:41.2	+40:56:09.6	13.930 ± 0.026	12.456 ± 0.018	11.597 ± 0.024
6	20:19:40.5	+40:56:25.3	14.118 ± 0.046	12.209 ± 0.032	11.315 ± 0.029
7	20:19:41.6	+40:55:45.5	14.405 ± 0.037	12.475 ± 0.030	11.212 ± 0.026
8	20:19:39.4	+40:56:23.7	–	12.610 ± 0.029	11.304 ± 0.025
9	20:19:39.2	+40:56:42.4	–	12.833 ± 0.032	11.414 ± 0.019

Note: Magnitudes satisfying the "read-flag" criteria of 1–3 are given for the sources.

(Hildebrand 1983), and d the distance to the source in kpc. We assumed a typical dust temperature of 20 K (see Tej et al. 2006; Klein et al. 2005). The flux densities were obtained from the JCMT-SCUBA maps shown in Fig. 5. To obtain the flux density of the entire cloud, we integrated up to the last contour (which is at 35% of the peak value). Using the above relation, we estimated dust masses of ∼7 and 15 $M_\odot$ from the 450 and 850 μm maps, respectively. Assuming a gas-to-dust ratio of 100, the above values translate to total masses of 700 and 1500 $M_\odot$ for the cloud from the 450 and 850 μm maps, respectively. We estimated the individual masses of the these two dust cores to be ∼250 (northern core) and 335 $M_\odot$ (southern core) from the 850 μm map. The cores are defined to cover regions upto ∼75% of the northern and southern intensity peaks. Exploring the range of T_d (20–40 K) and β (1–2), we infer that the mass estimates can be lower by up to a factor of ∼8.

In Fig. 6, we present the various components of the region associated with IRAS 20178+4046. The plot shows the contour map of the dust emission at 850 μm and the peak position of ionized gas emission at 1280 MHz overlaid on the 3.6 μm *Spitzer*-IRAC[4] image. As compared to the K_s-band image, the diffuse emission seen in the *Spitzer* image is far more extended. The outer envelope spreads out to a "hat-shaped" morphology. It is interesting to note that the southern core of the 850 μm map coincides with the radio continuum emission and the cluster of massive stars. One MIR source (G078.4373+02.6584 – $\alpha_{2000.0}$ = $20^h19^m39^s.4$; $\delta_{2000.0}$ = +40°56′35″.2) lies inside the southern core coincident with the radio peak position. The MSX MIR colours $F_{21/8}$, $F_{14/12}$, $F_{14/8}$, and $F_{21/14}$ of this source fall in the zone mostly occupied by compact HII regions (Lumsden et al. 2002). The MIR emission in UIBs due to PAH (see Appendix A) is also seen from this region. The morphology of the UIB emission is similar to what is seen in the *Spitzer* image. Comparing the FIR intensity maps of Verma et al. (2003), it is seen that this southern core is not spatially coincident with the FIR peaks at 150 and 210 μm but lies close to them (the core is located close to the last contours of the maps presented in their Fig. 5). It is likely that this is an evolved protocluster or a young (partly embedded) cluster where the massive stars develop UC HII regions and the cluster emerges from the parental cloud and the stars are detected in the NIR, whereas the northern

[4] The archival image presented is the Post-Basic Calibrated Data (PBCD) downloaded using the software Leopard. This work is based in part on observations made with the *Spitzer Space Telescope*, which is operated by the Jet Propulsion Laboratory, under NASA contract 1407.

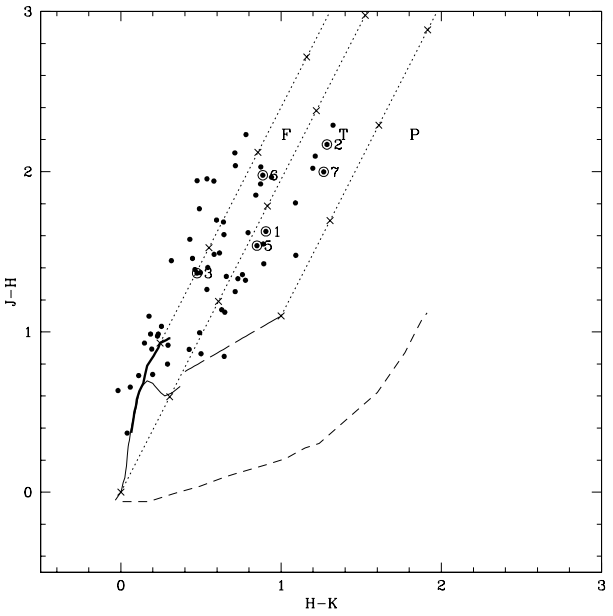

Fig. 4. Colour-colour diagram of the sources in the vicinity of the IRAS 20178+4046 region. The two solid curves represent the loci of the main sequence (thin line) and the giant stars (thicker line) derived from Bessell & Brett (1988). The long-dashed line is the classical T Tauri locus from Meyer et al. (1997). The parallel dotted lines are reddening vectors with the crosses placed along these lines at intervals of five magnitudes of visual extinction. We have assumed the interstellar reddening law of Rieke & Lebofsky (1985) ($A_J/A_V = 0.282$; $A_H/A_V = 0.175$ and $A_K/A_V = 0.112$). The short-dashed line represents the locus of the Herbig AeBe stars (Lada & Adams 1992). The plot is classified into three regions namely "F", "T", and "P" (see text for details). The colours and the curves shown in the figure are all transformed to the Bessell & Brett (1988) system.

core is only detected in the sub-mm. No radio emission (down to the level of the rms noise in the radio maps), MIR, or NIR emission is detected for this core. As seen clearly from Figs. 2 and 6, the northern core appears as an absorption region with a notable lack of stars. This northern core is relatively further away from the emission peaks in the two FIR bands (150 and 210 μm) as compared to the southern core. The mass of the two cores are similar, and they satisfy the mass limit criteria of 100 $M_\odot$ (Klein et al. 2005) for identifying the earliest stages of massive star formation. The above scenario suggests that this dense core could be harbouring a possible pre-protocluster or an early protocluster candidate where we are sampling the initial phases of cloud collapse in which massive stars have possibly begun to form deeply embedded in the cluster. Although the FIR data is not conclusive, the location of the sub-mm dust cores with respect to the other components most likely implies that we are seeing different evolutionary stages of star formation in the two cores. A similar massive star-forming complex IRAS 06055+2039 was studied by Tej et al. (2006) where the dense cloud core was at an earlier evolutionary stage compared to the associated HII region.

3.4. Line emission from the gas

Spectroscopic signatures from the interstellar gas around IRAS 20178+4046 were considered to explore additional information about this star-forming region. Millimetre-wave observations of CS(J = 2–1) by Bronfman et al. (1996), ^{13}CO(2–1) by Wilkins et al. (1989), and ^{13}CO(1–0) by McCutcheon et al. (1991) were translated to estimated gas mass of 544, 1130, and 1760 $M_\odot$ respectively, under reasonable assumptions. The lower value from the CS data is expected due to a smaller beam size (39″) used. These masses are similar to the estimates from the thermal emission from cold dust, 700–1500 $M_\odot$ (see Sect. 3.3). The available infrared spectroscopic measurements for IRAS 20178+4046 includes IRAS LRS data (covering 8 to 22 μm) and those by Faison et al. (1998) (covering 3–5.3 and 8–13 μm). The latter detected the [Ne II] line at 12.8 μm. We analysed the IRAS-LRS data to extract possible spectral signatures for the few selected ionic fine-structure lines commonly observed in HII regions. This resulted in clear detection of the [Ne II] line and marginal detections of the lines due to [S III] (18.7 μm) and [Ar III] lines (8.99 μm).

We explored a self-consistent model of the IRAS 20178+4046 region capable of explaining the observed infrared line emission, as well as radio continuum from the photo-ionized gas. The scheme developed by Mookerjea & Ghosh (1999) was used, which is based on the photoionization code CLOUDY (Ferland 1996). It considers various relevant physical and chemical processes involving constituents of the interstellar cloud. The geometrical parameters describing the cloud were taken from Verma et al. (2003), who successfully modelled the observed infrared SED and angular sizes using radiative transfer through the dust component. Our best model corresponds to a constant density cloud of radial dust optical depth, $\tau_{100\ \mu\mathrm{m}} = 0.005$ and a centrally embedded star cluster with an upper mass cut off of 17.5 $M_\odot$ (B0 type star) and the slope of the initial mass function of −1.6. The predicted radio emission at 1280 MHz is 51 mJy, in very good agreement with our GMRT measurement (57 mJy). The emerging infrared spectrum, including high-contrast lines, are presented in Fig. 7 along with the observed SED. The inferred luminosity of the [Ne II] line from the measurements of Faison et al. (1998) and IRAS LRS correspond to ∼74 and 5.3 $L_\odot$, respectively. This discrepancy could be due to the very different beams and spectral resolutions employed. The prediction of our model lies in between these two values at 26.1 $L_\odot$. The luminosities for the [S III] and [Ar III] lines extracted from IRAS LRS are 7.7 and 0.7 $L_\odot$ respectively, which are lower than predicted. However, the predicted line ratio [S III]/[Ne II] is very similar to the one from the LRS. Better measurements of these and other spectral lines are required to resolve the above issues. Several of the predicted lines (see Fig. 7) can easily be detected by the InfraRed Spectrograph (IRS) instrument onboard *Spitzer Space Telescope*, leading to better understanding of the star-forming complex associated with IRAS 20178+4046.

4. General star formation scenario in IRAS 20178+4046

The morphology of the radio emission of this UC HII region at higher resolution (Kurtz et al. 1994) is cometary in shape. As mentioned in Garay & Lizano (1999), the champagne flow and the bow-shock models explain the cometary morphologies satisfactorily, although it is difficult to differentiate between the two observationally. The morphology of the various components presented in Fig. 6 seems to suggest a champagne flow. In this model the medium in which the massive star is born has strong density gradients, which results in the HII region moving supersonically away from the high-density region in a so-called champagne flow (Garay & Lizano 1999). The HII region is density bounded and the pressurized HII gas bursts out of the cloud into a fan-like or plume-like structure. The presence of the dense

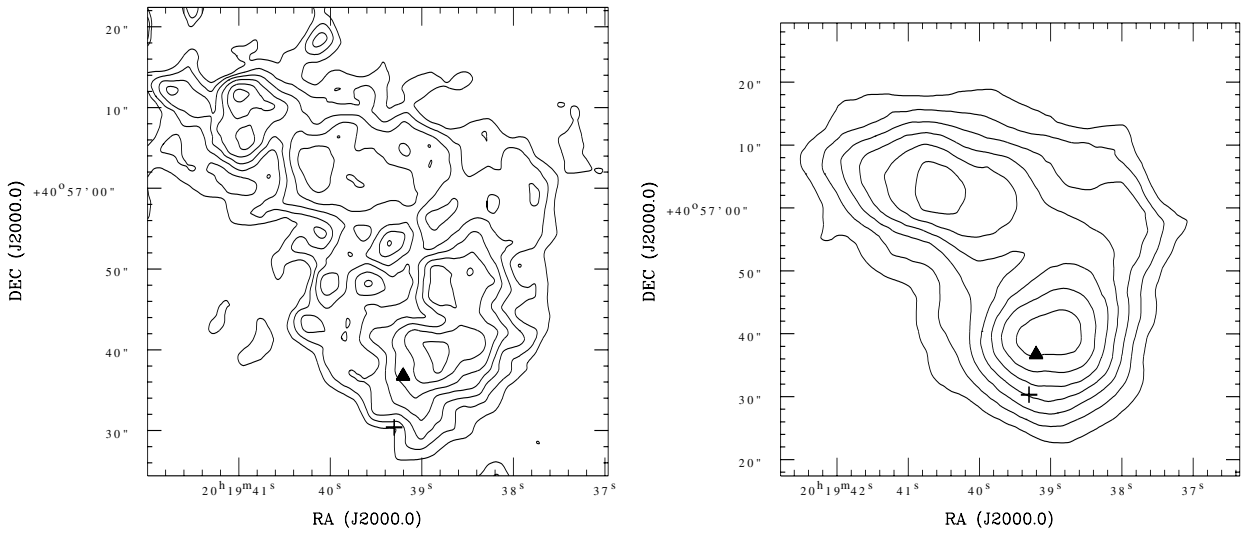

Fig. 5. Contour maps showing the spatial distribution of dust emission at 450 μm (*left*) and 850 μm (*right*) for the region around IRAS 20178+4046. The contour levels are at 35, 45, 55, 65, 75, 85, and 95% of the peak value of 4.19 and 1.72 Jy/beam at 450 and 850 μm, respectively. The FWHMs of the symmetric 2D Gaussian beams are 8.″8 and 14.″0 for the two wave bands. The plus sign and the filled triangle in each image mark the position of the IRAS point source and the radio peak, respectively.

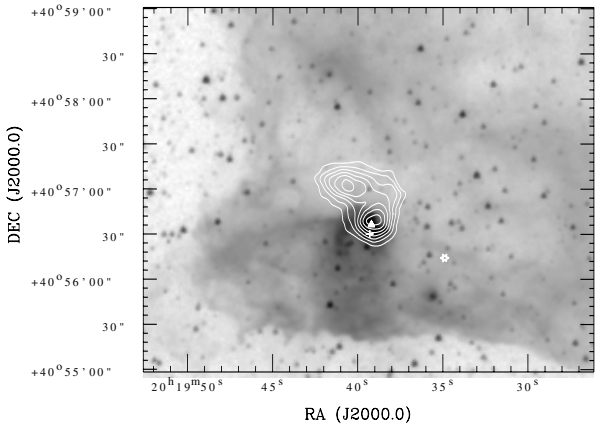

Fig. 6. Contour map of dust emission at 850 μm overlaid on the *Spitzer* 3.6 μm band image for the region around IRAS 20178+4046. The filled triangle shows the position of the radio peak, the plus sign marks the position of the IRAS point source, and the star marks the position of the FIR peaks at 150 and 210 μm (Verma et al. 2003).

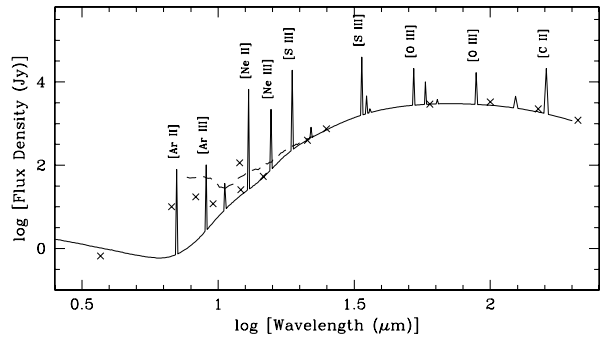

Fig. 7. The emerging spectrum (solid line) predicted by the model for IRAS 20178+4046. The dashed line represents the IRAS LRS from Volk & Cohen (1989). The crosses represent the photometric data taken from Verma et al. (2003), except for the 4 MSX bands that were estimated from respective maps.

dust core and the high density to the north of the UC HII region and the fan-like morphology seen in the *Spitzer* image and the MIR image adds strength to this conjecture. It is important to note that the fan-like morphology is also seen in the three other IRAC bands (4.5, 5.8, and 8 μm, which are not presented in this paper). Theoretical simulations in the champagne phase by Yorke et al. (1983) show that during this phase the resulting configuration is ionization-bounded on the high-density side and density-bounded on the side of the outward flow. The *Spitzer* image shows the presence of another high-density lane to the south of the fan-like diffuse emission. This southern high-density lane is spatially coincident with the east-west extended emission detected in the low-resolution 8.3 GHz map of Kurtz et al. (1999). Further high-resolution observations of the velocity structure of molecular gas in this star-forming region is crucial in understanding the details of the environment and the formation mechanism of the massive stars. In spite of the intrinsic temporal variability typically seen in masers (Stahler & Palla 2004) and the sensitivity of the single-dish observations carried out for this source, the absence of the OH maser could possibly be an indication of a more evolved HII region (Codella et al. 1994) in support of the optically thin scenario inferred from our radio observations.

5. Conclusions

The massive star-forming region associated with IRAS 20178+4046 has been studied in detail in the radio, infrared, and sub-mm wavelengths, leading to the following conclusions.

1. High-sensitivity and high-resolution radio continuum maps at 1280 and 610 MHz obtained from our observations using GMRT show a simple compact spherical morphology. The total integrated emission implies an exciting star of spectral type B0 – B0.5.
2. The sub-mm emission from cold dust was studied using JCMT-SCUBA at 450 and 850 μm, from which we estimate the total mass of the cloud to be ~700–1500 $M_{\odot}$, which is also supported by the estimates derived from the

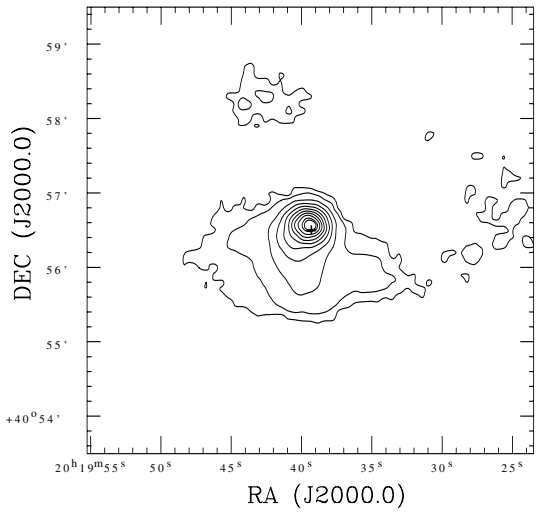

Fig. A.1. Spatial distribution of the total radiance in the UIBs for the region around IRAS 20178+4046 as extracted from the four MSX band images. The contour levels are at 5, 10, 20, 30, 40, 50, 60, 70, 80, 90, and 95% of the peak emission of 1.5×10^{-4} W m^{-2} Sr^{-1}.

millimeter-wave molecular line data. The 850 μm map shows two dense cores with masses ∼250 and 335 $M_{\odot}$. The southern core is most likely an evolved protocluster or a young cluster where the massive stars have formed the UC HII region and the cluster emerges out of the parental cloud. The northern core is only detected in the sub-mm and is a possible pre-protocluster.

3. The NIR colours from 2MASS data suggest the presence of several massive stars (earlier than ∼B0.5) within and enveloping the UC HII region, and they are likely to be deeply embedded.
4. The embedded star cluster has been characterised by modelling the observed radio continuum and infrared SED using a photoionization code. The upper mass cut off is found to be 17.5 $M_{\odot}$ (B0 type star) for a normal initial mass function.

Acknowledgements. We thank the anonymous referee for providing critical comments and suggestions, which have helped in improving the scientific content of this paper. We thank the staff at the GMRT who have made the radio observations possible. GMRT is run by the National Centre for Radio Astrophysics of the Tata Institute of Fundamental Research.

Appendix A: Spatial distribution of UIBs from the MSX data

We used the scheme developed by Ghosh & Ojha (2002) to extract the contribution of UIBs (due to the PAHs) from the MIR images in the four MSX bands. The scheme models the observations with a combination of thermal emission from the "normal" large interstellar dust grains (gray body) and the UIB emission from the gas component, under reasonable assumptions. The spatial distribution of emission in the UIBs with an angular resolution of ∼18″ (for the MSX survey) extracted for the region around IRAS 20178+4046 is shown in Fig. A.1. The morphology of the UIB emission is similar to that of the diffuse emission seen in the K_s-band and *Spitzer* images shown in Figs. 2 and 6. The integrated emission (upto 5% of the peak value) from the UIB features in band A (viz., 6.2, 7.7, 8.7 μm) and band C (11.3, 12.7 μm) is found to be 7.54×10^{-12} W m^{-2}. In comparison, the emission in the PAH bands (6.2, 7.7, and 11.3 μm) from the ISOCAM measurements is reported to be 1.87×10^{-12} W m^{-2} in Verma et al. (2003). Our higher value is not surprising considering that it includes two additional features and also covers a larger area. In addition, the spatial distribution of the warm dust component (optical depth; $\tau_{10\ \mu m}$) and its temperature (T_{MIR}) were generated (maps not presented here). The distribution of $\tau_{10\ \mu m}$ is compact with a peak value of 0.018, the peak coinciding with that of the UIB emission. On the other hand, T_{MIR} distribution is more extended ranging between ∼80–193 K, with the warmest region toward the western edge of extended UIB emission.

References

Baudry, A., Desmurs, J. F., Wilson, T. L., & Cohen, R. J. 1997, A&A, 325, 255
Bessell, M. S., & Brett, J. M. 1988, PASP, 100, 1134
Bronfman, L., Nyman, L. -A., & May, J. 1996, A&AS, 115, 81
Caswell, J. L., Murray, J. D., Roger, R. S., Cole, D. J., & Cooke, D. J. 1975, A&A, 45, 239
Chan, S. J., Henning, T., & Schreyer, K. 1996, A&AS, 115, 285
Codella, C., Felli, M., Natale, V., Palagi, F., & Palla, F. 1994, A&A, 291, 261
Codella, C., Felli, M., & Natale, V. 1996, A&A, 311, 971
Crowther, P. A., & Conti, P. S. 2003, MNRAS, 343, 143
Faison, M., Churchwell, E., Hofner, P., et al. 1998, ApJ, 500, 280
Ferland, G. J. 1996, Hazy, a brief introduction to CLOUDY, Univ. of Kentucky, Dept. of Phys. and Astron. Internal Reports
Garay, G., & Lizano, S. 1999, PASP, 111, 1049
Ghosh, S. K., & Ojha, D. K. 2002, A&A, 388, 326
Hildebrand, R. H. 1983, QJRAS, 24, 267
Klein, R., Posselt, B., Schreyer, K., Forbich, J., & Henning, Th. 2005, ApJS, 161, 361
Kurtz, S., Churchwell, E., & Wood, D. O. S. 1994, ApJS, 91, 659
Kurtz, S. E., Watson, A. M., Hofner, P., & Otte, B. 1999, ApJ, 514, 232
Lada, C. J., & Adams, F. C. 1992, ApJ, 393, 278
Lumsden, S. L., Hoare, M. G., Oudmaijer, R. D., & Richards, D. 2002, MNRAS, 336, 621
Mezger, P. G., & Henderson, A. P. 1967, ApJ, 147, 471
McCutcheon, W. H., Sato, T., Dewdney, P. E., & Purton, C. R. 1991, AJ, 101, 1435
Meyer, M. R., Calvet, N., & Hillenbrand, L. 1997, AJ, 114, 288
Mookerjea, B., & Ghosh, S. K. 1999, J. Astrophys. Astr., 20, 1
Ojha, D. K., Tamura, M., Nakajima, Y., et al. 2004a, ApJ, 608, 797
Ojha, D. K., Tamura, M., Nakajima, Y., et al. 2004b, ApJ, 616, 1042
Panagia, N. 1973, AJ, 78, 929
Price, S. D., Egan, M. P., Carey, S. J., Mizuno, D. R., & Kuchar, T. A. 2001, AJ, 121, 2819
Rieke, G. H., & Lebofsky, M. J. 1985, ApJ, 288, 618
Sandell, G. 2000, A&A, 358, 242
Schraml, J., & Mezger, P. G. 1969, ApJ, 156, 269
Slysh, V. I., Val'tts, I. E., Kalenskii, S. V., et al. 1999, A&AS, 134, 115
Stahler, S. W., & Palla, F. 2004, in The Formation of Stars, WILEY-VCH Verlag GmbH & Co. KGaA
Swarup, G., Ananthakrishnan, S., Kapahi, V. K., et al. 1991, Current Sci., 60, 95
Szymczak, M., Hrynek, G., & Kus, A. J. 2000, A&AS, 143, 269
Tej, A., Ojha, D. K., Ghosh, S. K., et al. 2006, A&A, 452, 203
Verma, R. P., Ghosh, S. K., Mookerjea, B., & Rengarajan, T. N. 2003, A&A, 398, 589
Volk, K., & Cohen, A. 1989, AJ, 98, 931
Wilking, B. A., Blackwell, J. H., Mundy, L. G., & Howe, J. E. 1989, ApJ, 345, 257
Yorke, H. W., Tenorio-Tagle, G., & Bodenheimer, P. 1983, A&A, 127, 313